PHYSICAL REVIEW C

NUCLEAR PHYSICS

THIRD SERIES, VOL. 5, NO. 5 May 1972

Radiative Electron Capture in ^{7}Be†

Börje I. Persson and Steven E. Koonin
California Institute of Technology, Pasadena, California 91109
(Received 21 January 1972)

The continuous spectrum of photons accompanying the electron-capture transition from ^{7}Be to the first excited state in ^{7}Li has been measured in coincidence with the nuclear γ rays from the deexcitation of this state. The end-point energy of the photon spectrum was determined to be 388 ± 8 keV, in good agreement with accepted mass differences. The probability of $1s + 2s$ radiative capture giving a photon energy greater than 50 keV per nuclear γ ray was determined to be $(10.3 \pm 0.6) \times 10^{-5}$. This result should be compared with the value 9.2×10^{-5} predicted by the theory of Martin and Glauber. At energies higher than 120 keV the shape of the spectrum agrees with the predictions of theory. At energies lower than 120 keV the intensity falls off faster than expected from the theory. Exchange and overlap corrections to the radiative-capture theory have been calculated and shown to be too small to account for the observed discrepancy.

INTRODUCTION

When an orbital electron is captured by a nucleus, there is a small probability that this process will be accompanied by the simultaneous emission of electromagnetic radiation. This effect, known alternatively as radiative capture or internal bremsstrahlung (henceforth denoted IB) was predicted by Morrison and Schiff.[1] The energy spectrum of the electromagnetic radiation was calculated to be continuous up to some maximum energy, the endpoint, and to have characteristic shape, with the process as a whole proceeding at a rate of about 10^{-4} of the ordinary nonradiative-capture rate.

Early attempts to experimentally verify the Morrison and Schiff theory were frustrated by the appearance of an excess of low-energy photons. This was explained in allowed captures by an improvement of the theory presented by Martin and Glauber[2,3] which included relativistic effects and the possibility of radiative capture from both s and p orbital states. While experimentally measured spectra have agreed well with the shape predicted by this theory, intensity measurements, relative to the ordinary nonradiative capture, have been made with poor accuracy. The present situation has been summarized elsewhere.[4-6]

A number of experiments have been published recently[7-9] in which the IB yield was found, with some accuracy, to be only 60–70% of what would be expected on the basis of Martin and Glauber's theory, suggesting that the theory is incorrect. This discrepancy motivated out experimental study of radiative electron capture. Accurate determinations of the intensity of bremsstrahlung are also relevant for experiments aimed at the determination of parity impurities in nuclear states through investigation of the circular polarization of nuclear γ rays.[10]

Because of the nature of the Martin and Glauber theory, its predictions were expected to be most accurate in elements of lowest Z, where radiative capture from p states is expected to be small, as are relativistic effects and effects due to the nuclear charge. We therefore decided to investigate IB from allowed electron capture in the element of lowest possible Z, that of ^{7}Be. This nucleus decays through only $1s$ and $2s$ capture, thus eliminating complications due to p-state capture. Ap-

proximately 10% of the captures go to the 477-keV state of ^{7}Li, with subsequent emission of a nuclear γ ray. We used this γ ray to perform an IB-γ coincidence experiment. Because the probability for internal conversion of the γ ray is negligibly small, the number of IB quanta per nuclear γ ray is equivalent to the ratio of probabilities for total radiative and total nonradiative electron capture to the 477-keV state in ^{7}Li.

EXPERIMENT

In the experiment, we attempted to measure the bremsstrahlung in one NaI scintillation counter coincident with the occurrence of total absorption of the nuclear γ ray in a second scintillation counter. As the probability of radiative capture is small, the experiment had to be optimized subject to the following:

(a) Random coincidences had to be kept to a small fraction of the true IB-γ coincidences, so that corrections for such randoms could be done with confidence. This seems not to have been the case in the previous experiment,[9] where at best the rate of random events was 300% of the rate of true events. This optimization of the true-to-random ratio called for the shortest possible resolving time of the coincidence apparatus. However, this requirement was in conflict with the desire to maintain 100% coincidence efficiency over the widest possible energy range. In order to fulfill these conflicting requirements, we chose two-parameter analysis; i.e., both the energy of the bremsstrahlung quantum and the time of arrival in its detector, relative to the arrival time of the γ ray in its detector, were measured simultaneously.

(b) In order to further reduce the random rate, it was necessary to use the weakest possible source, while simultaneously keeping the time required for data accumulation within reason. These conditions forced us to use the most efficient detector geometry.

(c) A choice of geometry had to be made with awareness of the possibility of scattering taking place from one detector to another. Such events would have caused false prompt events to be superimposed on the bremsstrahlung data.

The detector arrangement is shown in Fig. 1. The collimating lead shield was introduced to reduce scattering events between the crystals. The angles of its cones were chosen to cover the full face of each detector at the mean absorption depth of the radiation it was designed to measure. It might appear that backscattering would have been significant for this face-to-face arrangement, and so an arrangement with the detectors at 90° from one another should have been chosen. In a backscattering event, however, the full energy of the γ ray is not registered in the detector. Therefore, such events can be discriminated against electronically. As will be seen, the experimental spectra confirm the hypothesis that prompt events due to backscattering were negligible. Also, a 90° geometry greatly reduces geometrical efficiency, requiring much longer counting times for a given true-to-random coincidence ratio. For these reasons, the face-to-face geometry was chosen. In order to further reduce prompt unwanted events, we found it advantageous to introduce a copper plate between the source and the γ detector to absorb escaped iodine x rays. A cadmium lining on the side of the lead collimator facing the IB detector was used to reduce detection of x rays from the lead.

Great care was taken to minimize background levels. The entire detector system was enclosed in 2 in. of iron bricks, which were chosen instead of lead because of their low natural radioactivity. Surrounding the iron house was a layer of $\frac{3}{4}$-in. plastic scintillator covering >80% of the 4π sr surrounding the detectors. This served as anticoincidence shielding and reduced prompt coincidences due to cosmic rays scattered through the building. 4 in. of lead surrounded the plastic scintillators. The collimator and iron house were constructed to ensure accurately reproducible positioning of the source and detectors. With these precautions, the background prompt coincidence rate measured in the system with no source was reduced to 3 or 4 counts/h, as compared with the ~100 IB-γ coincidences per hour obtained with the source strengths used.

Sources were prepared from commercially obtained $^7BeCl_2$ by evaporating a small drop on cellophane tape and sealing with a second piece of tape.

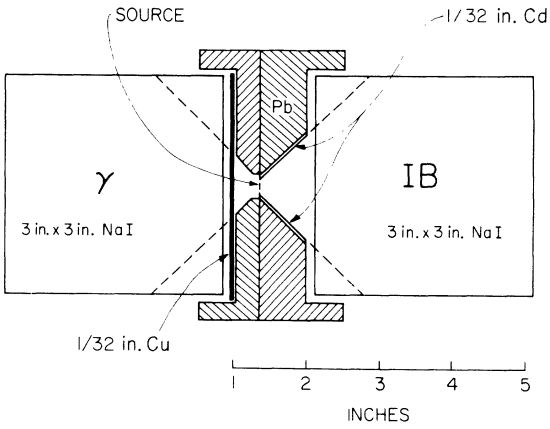

FIG. 1. Scale drawing of the experimental arrangement of the detectors.

Care was always taken to make the source spot considerably smaller than the $\frac{1}{8}$-in. hole in the collimator, thereby preventing inaccurate results due to partial shielding of the source. The sources were checked for impurities with a high-resolution Ge(Li) detector and were found to be free of any extraneous γ rays of energy between 0.5 and 3.5 MeV to better than 0.1 ppm. Source strengths were chosen to give a counting rate of about 3500 sec^{-1} in the geometry used.

In order to obtain the best possible time resolution with the two 3-in. × 3-in. Harshaw integral line NaI detectors employing RCA 8054 photomultiplier tubes, these were operated at highest possible voltages (~2500 V) consistent with stable operation. The voltage was distributed to obtain minimum spread in transit time. Timing pulses were generated by fast pulse-height discriminators, lower-level discriminators (LLD), set at as low a level as possible without undue dead time due to triggering by noise pulses. In this way, time jitter due to variations in pulse amplitude was minimized.

As is shown in the block diagram of the electronics in Fig. 2, a second fast discriminator, upper-level discriminator (ULD), was included in each of the fast branches. The triggering level of this discriminator was set high enough (~30 keV for the IB branch and ~350 keV for the γ branch) to reject noise pulses. The short output pulses from the two discriminators in each branch were fed to an AND gate whose output was timed by the corresponding LLD. These AND gates generated start and stop pulses for the time-to-amplitude converter (TAC). With these two features, high voltage and dual discriminators, resolution was approximately $2\tau = 4.0$ nsec for energies >250 keV and $2\tau = 6.0$ nsec for an IB energy of 100 keV.

Because of the variation in pulse height with energy, the time spectrum changed shape and position considerably for varying energies in the IB detector, as can be seen in Fig. 3. For this reason we chose to employ a TAC and two-parameter analysis, which allowed us to record time spectra for all IB energies and eliminated the need for a wide time window, which would have been necessary to maintain 100% coincidence efficiency at low energies. This method offered the additional advantage that the random coincidences were recorded concurrently with the prompt ones.

The TAC received start pulses from the γ branch and stop pulses from the IB branch, the latter delayed by about 50 nsec to place prompt events in the center of the TAC range. The TAC also generated others signals besides the output. A valid start signal indicated a pulse had been received from the γ branch and time analysis had begun. Any pulse from the IB branch arriving within ±50 nsec would then cause an output, along with a valid stop signal. Single-channel analyzers (SCA) were inserted in the slow γ branch and were set to trigger on the photopeak of the γ line. Valid starts in slow coincidence with the output signal from the SCA drove a scaler, which recorded the number of times a γ pulse caused the system to begin looking for an IB pulse. This number was used for the final normalization. Valid stop signals in coincidence with the SCA signal opened the gate of the two-parameter analyzer. Care was taken to adjust the TAC and the analyzer so as to include all prompt events above 30 keV within the range of time analysis. To eliminate scaler counts

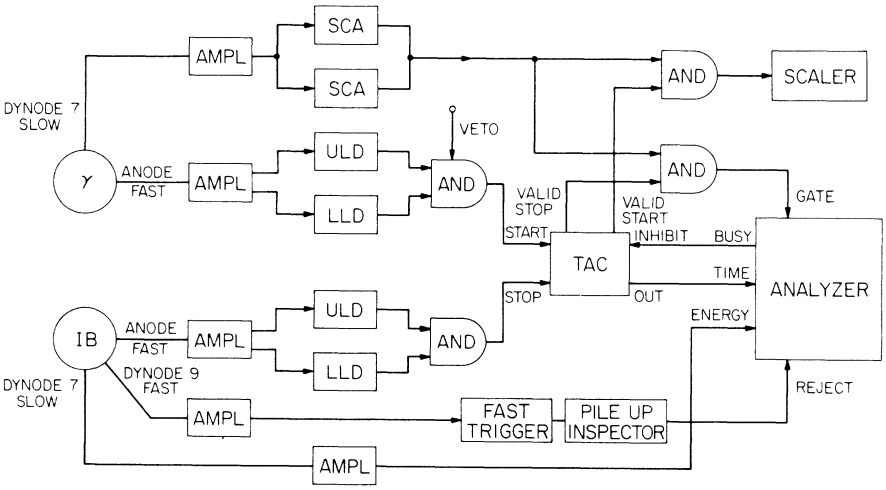

FIG. 2. Block diagram of the electronics. The veto signal is derived from the anticoincidence shield. Modular units from Edgerton, Germeshausen, & Grier, Inc., Salem, Massachusetts, were used for the fast system.

accumulated during the time the analyzer was busy, which would destroy the normalization, the entire system was gated off while analysis proceeded.

A pileup rejection system was employed to reduce distortion of the pulse-height spectrum in the IB branch. It prevented the pileup of pulses separated by more than 130 nsec, provided their amplitudes exceeded 70 keV.

The parallel SCA's in the γ branch were employed in a technique to correct for prompt background. It was desired to record only those coincidences that corresponded to total absorption of the 477-keV γ line in the γ branch. It was therefore necessary to eliminate all coincidences that were related to a possible continuum under this photopeak. Data were first taken with both windows superimposed upon one another and on the photopeak. Background data, which were to be subtracted, were then taken with the two windows split, one above the peak and one below, with the idea that the continuum counts in the region of the photopeak would be averaged by the two windows. Some true IB counts were also recorded in the run with split windows. However, correction for these was effected by subtracting the normalizing scaler counts, as well as the actual spectrum.

Two sets of data were accumulated, each for about 14 days. Different samples of ^{7}Be were used for these sets, and in one run the source employed was about twice as strong as in the other. Only one set of data, that accumulated with the stronger source, was obtained using the copper absorber described earlier. Each set of data was analyzed independently, and since the results were consistent, the two sets were summed and analyzed together.

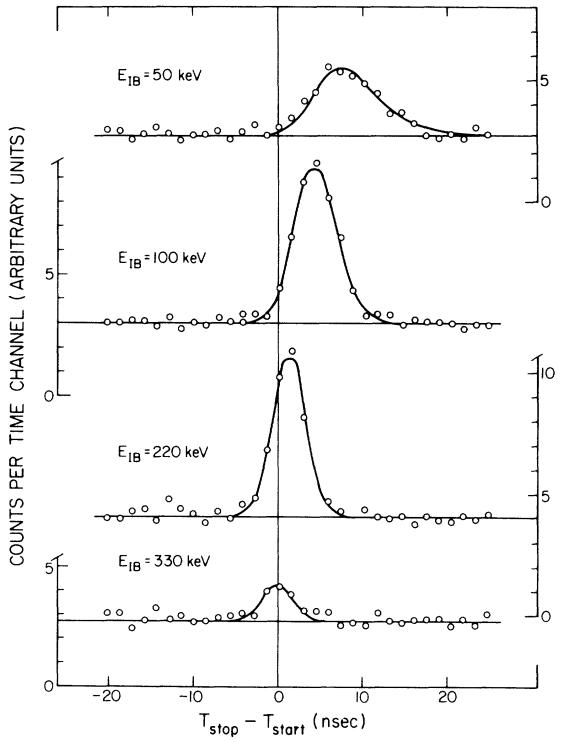

FIG. 3. Time spectra for representative pulse heights from the IB detector. The curves result from least-squares adjustments of the intensities of the time spectra obtained with a ^{22}Na source. The variation with energy of the background level of random events reflects the Compton distribution of the γ line, while the variation of the area of the peak above the random level reflects the IB spectrum. The data shown were obtained with the stronger of the two sources used. With the weaker source the ratio of the peak height to random level was about twice as large.

DATA ANALYSIS

The raw data for each run consisted of two sets of 128 32-channel time spectra, one set of actual IB data, and one set of split-window background. The background spectra, after normalization of counting times, were subtracted from the IB data to correct for any spurious coincidences, as explained previously. This resulted in 128 32-channel time spectra, each consisting of a prompt peak whose shape and position varied with energy, and a background due to random coincidences, whose variation in energy was expected to follow a ^{7}Be pulse-height spectrum. In order to obtain a well-determined shape of the prompt "ridge" in the energy-time plane, a similar two-dimensional spectrum of annihilation radiation was obtained using a ^{22}Na source placed in the experimental geometry, with absorbers used to stop the positrons close to the source. As practically all the detected radiation from ^{22}Na is in coincidence, each ^{22}Na time spectrum contained only the prompt peak, the random background being almost entirely absent. The ^{22}Na spectra were used to separate the ^{7}Be prompt events from the random events by a least-squares adjustment of each ^{22}Na time spectrum, plus a constant background. In this way the number of prompt events in each energy channel was determined.

The results of this separation are shown in Fig. 4. The prompt events appearing at the energy of the photopeak are disturbing, and we cannot account for them satisfactorily. However, possible origins will be discussed later. It is therefore an open question whether the peak has an associated Compton distribution. In the subsequent data analysis we assumed its presence. In any event, it is small, as shown in Fig. 4, and affects the IB determination little.

Correction for the efficiency of the fast-coincidence system was applied to the data. The very unlikely possibility of a deviation from 100% efficiency of the slow-coincidence system, i.e., the SCA's, was disregarded, as it canceled the normalization of the IB to the scaler counts. The coincidence efficiency of the fast system was measured using the annihilation radiation from ^{22}Na by recording two one-dimensional spectra. The first was taken with the source in the experimental geometry, and gated exactly as the IB measurements were, i.e., by requiring both a SCA pulse and a valid stop. It differed from the spectrum used to define the prompt ridge only by the fact that the TAC output pulses were not analyzed. The second spectrum was identical to the first, save for the fact that the gating condition of a valid stop was relaxed, so that a SCA pulse by itself was sufficient to open the gate. As random coincidences were, for practical purposes, absent, a ratio of these two spectra gave the coincidence efficiency of the fast system. In this way, coincidence efficiency was found to be 100% to below 100 keV, with a fall off to 90% at about 50 keV. A check of the measurement of the coincidence efficiency was obtained by taking the ratio of the random background spectrum, found during the process of prompt-peak separation, to an ungated ^{7}Be spectra taken in the experimental geometry. This gave results identical to those obtained with ^{22}Na.

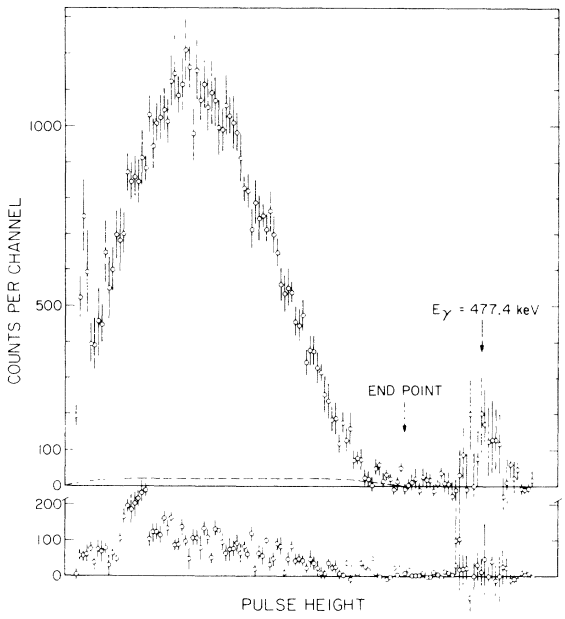

FIG. 4. Pulse-height spectra of prompt events. The top spectrum is the sum of the IB data from both runs corrected for prompt background by the split-window technique described in the text. The spectrum corresponds to 3.734×10^{9} scaler counts. The bottom spectrum is one of the spectra obtained with the windows split, normalized to the same counting time as the top spectrum. The majority of the pulses in the bottom spectrum are due to bremsstrahlung, which appears because the split windows covered the wings of the 477-keV peak. In the top spectrum, the Compton distribution associated with the peak at the γ-ray energy is indicated as a dashed curve. The peak at the lowest energies is associated with the 29-keV iodine x rays counted during the run without the copper absorber.

Correction for the response function of the detector was applied next. For this purpose, pulse-height spectra from a number of calibration sources emitting single γ lines (^{170}Tm, 84 keV; ^{141}Ce, 145 keV; ^{203}Hg, 279 keV; ^{51}Cr, 320 keV; ^{113}Sn, 393 keV; ^{7}Be, 477 keV; ^{85}Sr, 514 keV; and ^{137}Cs, 662 keV) were obtained using the experimental geometry. Because a comparatively large NaI crystal was used, and the γ-ray energies of interest do not extend beyond 500 keV, the peak-to-total ratio was large, so that an approximate form of the Compton continuum could be used. Two functional forms were used: either a rectangle or a trapezoid. The pulse-height distributions from the calibration sources were used to determine the energy dependence of the functional parameters. Corrections were applied to the ^{7}Be IB pulse-height spectrum using the peel-off method, i.e., starting at the highest energies and successively subtracting the Compton distribution due to each channel.

Because of the complex experimental geometry, the total efficiency of the detector could not be reliably calculated. This necessitated the determination of this function in a somewhat involved manner. A spectrum for each calibration source was taken with the source 3 in. above, and on the axis of, the NaI crystal. As the total efficiency of the detector in this configuration is easily calculable from tabulated[11] absorption coefficients, the absolute source strengths could be determined. The areas of the spectra taken in the experimental geometry then gave the efficiency of the crystal in the experimental arrangement at the calibration energies. Corrections were made for absorption in materials encapsulating the crystal.

At this point, a correction for escaped iodine x rays was applied. It was negligible above 50 keV.

The nonrelativistic Morrison and Schiff theory predicts a differential spectrum of the form $N(E) = AE(E_0 - E)^2$, where A is a constant, E is the energy of the radiated photon, and E_0 is the end point. The relativistic theory gives essentially the same form, though A now becomes a slowly varying function of energy. If $\sqrt{N(E)/E}$ is plotted as a function of E (Jauch plot), it should be very close to a straight line, with the zero crossing giving

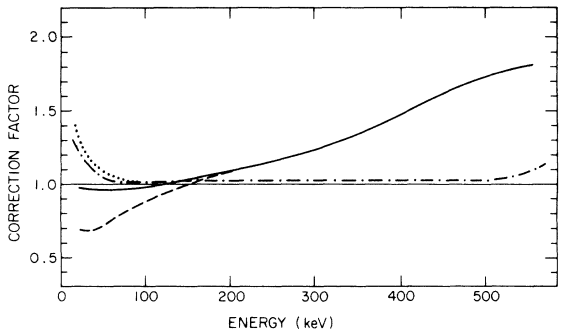

FIG. 5. Corrections applied to the pulse-height distribution to convert it into the spectrum of photons: coincidence efficiency (• • •), trapezoidal response function (——), rectangular response function (---), and total detector absorption (-•--•-).

the end-point energy.

A Jauch plot of the spectrum obtained after the mentioned corrections had been imposed on it was constructed and the end point was determined by fitting a straight line over the energy range 130–340 keV. Using this end point, a theoretical spectrum was computed and smeared using Gaussian peaks whose width variation with energy corresponded to the resolution variation of the detector. A correction factor for resolution was thus determined and applied to the data. It was found to be negligibly small except at the very highest and lowest energies, thus validating the end-point determination made before resolution correction.

Correction factors for coincidence efficiency, Compton continua (including peak-to-total ratio), and detector efficiency are shown in Fig. 5. Note that the detector efficiency was almost constant. This was due to the fact that while the absorption in the NaI decreased as energy increased, scattering and penetration in the collimator increased, thus compensating for the drop in absorption by enlarging the effective solid angle.

RESULTS

The results of the present experiment, as well as previous results of Lancman and Lebowitz,[9] are summarized in Table I. Values are given for the bremsstrahlung intensity per γ ray, which were obtained by summing the experimental spectrum over the indicated energy intervals. The table gives the results obtained with each one of the two approximations for the response function used in the peeling of the pulse-height spectrum. The average of these results was taken as the final result and half of the difference between them was taken as the error caused by the use of these approximations for the response functions.

Figure 6 shows the fully corrected total bremsstrahlung spectrum, as well as the corresponding Jauch plot. On the Jauch plot is also the line of best fit in the region 130–340 keV. From the slope of this line, it is possible to determine the total bremsstrahlung intensity over the whole energy range of the spectrum, assuming the shape to be essentially given by the theory of Morrison and Schiff. Even in the fully relativistic theory, though, the deviation from a straight line over this region is at most 0.5%. We therefore show on the experimental IB spectrum a spectrum whose shape is given by the Martin and Glauber theory, and whose normalization was adjusted to match that obtained from the slope of the Jauch plot. In computing the Martin and Glauber spectrum, an end point of 384 keV obtained from the latest mass tables[12] was used, as this is more accurate than our determination. A value[13] of 0.033 was used for the L/K capture ratio, which does not include corrections for exchange and overlap effects.[14]

TABLE I. The results of the present experiment compared with the predictions of the theory and the results of Ref. 9.

	Energy range (keV)	Present results Experiment[a] A	B	C	Theory	Results of Ref. 9[b] Experiment	Theory
$\frac{IB}{\gamma}\times 10^5$	120–360	7.8	7.6	7.7±0.5	6.4	4.9±1.0	7.0
	100–360	8.8	8.5	8.6±0.5	7.3		7.4[c]
	50–360	10.6	10.0	10.3±0.6	9.2		
	0–384[d]	12.6	12.5	12.6±0.9	10.0		
End point (keV)		388	387	388±8	384[e]	395±25	

[a] Column A (B) corresponds to the use of trapezoidal (rectangular) response functions. Column C gives the averages of the entries of Columns A and B.

[b] The value of IB/K capture was converted to IB/γ using the value 0.124 for the L/K capture ratio.

[c] The value 7.4 was obtained from the corresponding value in Ref. 9 after modifications described in the text.

[d] The values correspond to a linear Jauch plot least-squares-adjusted to the data over the energy range 130–340 keV.

[e] Value obtained from mass differences, Ref. 12.

From this L/K capture ratio, we compute a screening factor ratio S_{2s}/S_{1s} of 0.26.

The most significant systematic errors in the values for the bremsstrahlung per γ ray listed in Table I are related to the determination of the detector efficiency, the uncertainty in whether or not the peak near 477 keV is accompanied by a Compton continuum, and the approximate form of the response functions. In the mentioned order, they were estimated to be 3%, 3%, and 2 to 4%, the latter value being dependent upon the energy range. The rms value of these errors and the statistical error of about 1% is 6%, and corresponds to the errors given in the table.

Various explanations in terms of scattering between the detectors combined with random time overlap of pulses, were attempted to account for the appearance of the peak in the prompt pulse-height spectrum near the γ-ray energy. Such events could account for less than 10% of the observed intensity. Furthermore, any scattering events which might occur would be accompanied by a peak in the prompt spectrum at the energy ($\approx$170 keV) of the backscattered nuclear γ ray. Since there is no evidence for such a peak (cf. Fig. 4) in either the bremsstrahlung or the split-window background spectra (where it would have been enhanced), scattering events can be discounted. The energy range of the IB detector was extended to 2 MeV in a supplementary measurement. No additional peaks could be detected, ruling out possible contributions from γ cascades.

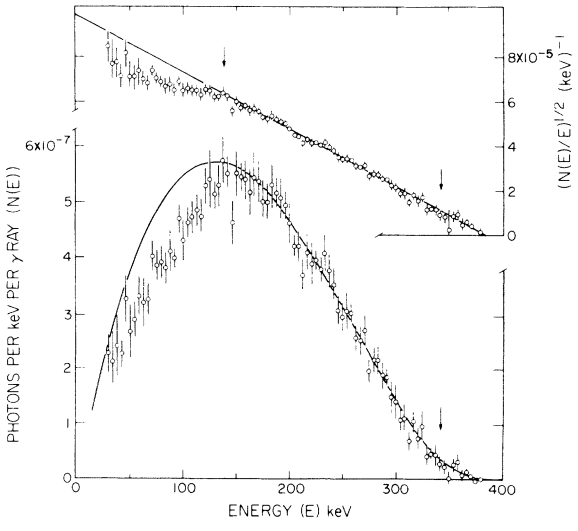

FIG. 6. Fully corrected IB spectrum obtained by peeling using the trapezoidal response function, and the corresponding Jauch plot. The straight line on the Jauch plot is the best fit for the interval between the arrows (130–340 keV). The curve on the IB spectrum is the theoretical spectrum which corresponds to this line.

DISCUSSION

The total yield of IB per nuclear γ ray is given, in the notation of Martin and Glauber, by

$$\frac{\omega_{IB}}{\omega_\gamma} = \frac{\omega_{1s}+\omega_{2s}}{\omega_K+\omega_L} = \frac{\omega_{1s}}{\omega_K}\,\frac{1+\omega_{2s}/\omega_{1s}}{1+\omega_L/\omega_K}\,, \tag{1}$$

with

$$\frac{\omega_L}{\omega_K} = X^{L/K}\,\frac{q_{2s}^{\,2}}{q_{1s}^{\,2}}\,\frac{|\psi_{2s}(0)|^2}{|\psi_{1s}(0)|^2} \tag{2}$$

and

$$\frac{\omega_{2s}}{\omega_{1s}} = F\,\frac{|\psi_{2s}(0)|^2}{|\psi_{1s}(0)|^2}\,. \tag{3}$$

Here ω_{1s} is the rate of radiative $1s$ capture, ω_K is the rate of nonradiative K capture, etc., Ψ is the electron wave function, and q is the neutrino momentum. Since the difference in binding energies between the $1s$ and $2s$ states in ^{7}Be is negligible in comparison with the transition energy, we are justified in setting $q_{1s} = q_{2s}$. The factor $X^{L/K}$ is the exchange and overlap correction of Bahcall,[14] which arises from considering antisymmetrization of the wave function and the change in nuclear charge. For Be, $X^{L/K} \approx 3.7$. As these effects are not considered in the Martin and Glauber theory, we set $X^{L/K} = 1$ in order to consistently treat the electronic wave functions in the same approximation. The numerical factor F has a dependence upon the energy range considered, and should ideally include similar corrections to the Martin and Glauber theory for exchange and overlap effects. As is demonstrated in the Appendix, the inclusion of exchange and overlap effects in both the theory for the radiative- and the theory for the nonradiative-capture processes has practically no effect on the ratio $\omega_{IB}/\omega_\gamma$. In the absence of these effects, the factor F is determined solely by the nonequality of the relativistic corrections to $1s$ and $2s$ capture, and is therefore close to unity. Actually, for the total energy range, $F = 1.00$. With these approximations, we have for ^{7}Be

$$\omega_{IB}/\omega_\gamma = \omega_{1s}/\omega_K\,. \tag{4}$$

A comparison of the present experimental results with this approximation to the theory shows that over the largest energy range accessible in this measurement (50 to 360 keV), the intensity of the bremsstrahlung is in fair agreement with the theoretical prediction.[15] However, there is a noticeable difference in the shapes of the spectra, showing an apparent experimental excess of high-energy photons and a corresponding deficiency at low energies.

In comparison of the present results with those of Lancman and Lebowitz,[9] some care should be taken. The latter experimental value is given as bremsstrahlung intensity per K capture, computed using an L/K ratio of 0.124. We have therefore decreased this experimental number by 12%. In adjusting the latter theoretical value, we have assumed that ω_{1s}/ω_K and ω_{2s}/ω_K were computed from the Martin and Glauber theory and summed. We therefore have decreased the published theoretical number by 3%, corresponding to an L/K capture ratio of 0.033, in order to convert this theoretical number to bremsstrahlung per nuclear γ ray. In addition, Lancman and Lebowitz[16] used a screening factor ratio of 0.5 in calculating the ratio ω_{2s}/ω_{1s}, while a screening factor ratio of 0.26 gives a relative contribution of 3%. We have therefore further decreased the theoretical number by 3%. The residual discrepancy appearing in Table I might be due to the use of the experimentally determined end point, 395 keV, in computing the theoretical number, rather than the more accurate 384 keV obtained from the mass tables.

When this experiment began, it was assumed that elements of lowest Z would follow the Martin and Glauber theory most closely, because of approximations made in the theory during the treatment of the Coulomb field. However, the relative change of the nuclear charge during the capture process is large for low-Z elements, and so one might expect that corrections to the Martin and Glauber theory, similar to those applied by Bahcall to the nonradiative-capture theory, would be of importance. Indeed, the factor F in Eq. (3) changes, for the total range of the spectrum, from 1.00 to 2.9 as the result of these corrections (see Appendix). However, the inclusion of these effects in both the radiative- and nonradiative-capture theories leaves the ratio $\omega_{IB}/\omega_\gamma$ unchanged to within 0.1% and does not explain the deviations of our experimental results from the Martin and Glauber theory.

In Be, the $2s$ electrons participate in chemical binding, and so one might expect the capture processes to be dependent on the chemical environment. The half-life of ^{7}Be has been shown[17] to depend to about one part in 10^3 on the chemical surrounding of the nucleus. While the half-life (and ω_γ and ω_{IB}) is proportional to the electron density at the nucleus, the ratio $\omega_{IB}/\omega_\gamma$ would be dependent on the charge density only in second order. Since the range of the Green's function is only 5% of the Bohr radius of Be at the photon energy of 100 keV and decreases with increasing photon energy, chemical effects on the relative rates of radiative and nonradiative capture are expected to be negligibly small.

APPENDIX

Proper consideration of the change in nuclear charge during the capture process results in two corrections to the Martin and Glauber theory: modification of the Coulomb Green's operator, and exchange-overlap corrections similar to Bahcall's for nonradiative capture. Both of these corrections, however, will be shown to have a negligible effect on the ratio $\omega_{IB}/\omega_\gamma$ for the range of energies investigated in this experiment.

In their treatment, Martin and Glauber have used the Coulomb Green's operator,

$$G_E(\vec{r},0)=\sum_\beta \frac{\psi_\beta(\vec{r})\psi_\beta^*(0)}{E_\beta - E},$$

making the assumption that captures from occupied states followed by radiative transitions contribute terms equal to those corresponding to virtual transitions to occupied states followed by capture, which are forbidden by the exclusion principle. This, however, is not completely valid. Radiation before capture takes place in the Coulomb field of element Z, while radiation following capture takes place in the field of element $Z-1$. This, in turn, implies for Be that the term in the Green's function corresponding to the occupied $2s$ state is incorrect, as this radiative matrix element must be evaluated using wave functions of Li. However, distortion of the spectrum would be expected to occur only at the lower photon energies ($k< Z\alpha m \approx 20$ keV for Be), where the poles corresponding to the bound states contribute strongly to the transition amplitude.

Exchange-overlap corrections can be applied to the Martin and Glauber theory in a manner analogous to Bahcall's procedure for obtaining $X^{L/K}$. In computing the rate of radiative $1s$ capture, the square of the matrix element $|M_{1s}(\vec{k},\vec{p})|^2$ given by Eq. (3.11b) of Ref. 3 should not be used in Eq. (2.31) of Ref. 2, but rather one should use the square of the exchange-corrected matrix element, $|M_{1s}^{ex}(\vec{k},\vec{p})|^2$, given by

$$|M_{1s}^{ex}(\vec{k},\vec{p})|^2=\left|\langle 2s'|2s\rangle M_{1s}(\vec{k},\vec{p})-\langle 2s'|1s\rangle M_{2s}(\vec{k},\vec{p})\right|^2 + \sum_{n\geq 3}|\langle ns'|2s\rangle|^2|M_{1s}(\vec{k},\vec{p})|^2,$$

where the unprimed (primed) states denote the electronic wave functions in ^{7}Be (^{7}Li). The various terms in this expression have a physical interpretation similar to the corresponding terms in the nonradiative-capture theory.[14] The first term is an interference between two processes: radiative capture of a $1s$ electron in ^{7}Be with the $2s$ electron in ^{7}Be remaining a $2s$ electron in ^{7}Li, and radiative capture of a $2s$ electron in ^{7}Be with the $1s$ electron in ^{7}Be becoming a $2s$ electron

in ^{7}Li. The two processes interfere with a minus sign because of the necessary antisymmetrization of the electronic wave functions. The summation corresponds to all those processes in which the $1s$ electron undergoes radiative capture and the $2s$ electron in ^{7}Be jumps to some state in ^{7}Li. The terms add incoherently as they differ in final state. The $1s'$ term is excluded from the summation as it leads to $2s$ radiative capture, and the $2s'$ term is excluded as it has been accounted for in the interference term. Using closure of the s' states, the summation can be written as

$$(1-|\langle 1s'|2s\rangle|^2-|\langle 2s'|2s\rangle|^2)\,|M_{1s}(\vec{k},\vec{p})|^2\,.$$

Strictly speaking, the energy-conserving δ function in Eq. (2.31) of Ref. 2 should include the binding energies of the electronic states, which will modify the phase-space factors slightly. As the binding energies are only of the order of 100 eV, and projections of $|2s\rangle$ on high-lying continuum states of ^{7}Li are expected to be very small, the binding energies can be disregarded.

This antisymmetrization of the wave function then implies that the new relativistic correction, $R_{1s}^{\rm ex}(k)$, is given by

$$R_{1s}^{\rm ex}(k)=\tfrac{1}{2}[(A_{1s}^{\rm ex})^2+(B_{1s}^{\rm ex})^2 + (1-|\langle 1s'|2s\rangle|^2-|\langle 2s'|2s\rangle|^2)(A_{1s}{}^2+B_{1s}{}^2)]\,,$$

where

$$A_{1s}^{\rm ex}=\langle 2s'|2s\rangle A_{1s}-\langle 2s'|1s\rangle A_{2s}\frac{\psi_{2s}(0)}{\psi_{1s}(0)}\,,$$

$$B_{1s}^{\rm ex}=\langle 2s'|2s\rangle B_{1s}-\langle 2s'|1s\rangle B_{2s}\frac{\psi_{2s}(0)}{\psi_{1s}(0)}\,,$$

and A_{1s} and B_{1s} are given by Eqs. (3.12a) and (3.12b) of Ref. 3. Similar expressions for $2s$ capture are obtained by interchanging the symbols $1s$ and $2s$ in the states of ^{7}Li and ^{7}Be. Since $\psi_{1s}(0)/\psi_{2s}(0)$ is large, $A_{2s}^{\rm ex}$ and $B_{2s}^{\rm ex}$ may differ considerably from A_{2s} and B_{2s}. It should be noted that the summation over electron spins and neutrino and photon polarizations and averaging over nuclear orientations need not be repeated as a consequence of these corrections. This is due to the fact that, neglecting mixing of the $2s_{1/2}$ and $2p_{1/2}$ levels, which is small in ^{7}Be, the matrix structures of M_{1s} and M_{2s}, as given by Eq. (3.11b) of Ref. 3, are identical.

In the same approximation, similar expressions can be written for the K and L capture rates. Instead of writing

$$\omega_\gamma=\omega_K+\omega_L\propto|\psi_{1s}(0)|^2+|\psi_{2s}(0)|^2\,,$$

one should write

$$\omega_\gamma=\omega_K^{\rm ex}+\omega_L^{\rm ex}+\omega_0^{\rm ex}$$

with

$$\omega_K^{\rm ex}\propto|\langle 2s'|2s\rangle\psi_{1s}(0)-\langle 2s'|1s\rangle\psi_{2s}(0)|^2\,,$$

$$\omega_L^{\rm ex}\propto|\langle 1s'|1s\rangle\psi_{2s}(0)-\langle 1s'|2s\rangle\psi_{1s}(0)|^2\,,$$

and

$$\omega_0^{\rm ex}\propto(1-|\langle 2s'|2s\rangle|^2-|\langle 1s'|2s\rangle|^2)|\psi_{1s}(0)|^2 + (1-|\langle 1s'|1s\rangle|^2-|\langle 2s'|1s\rangle|^2)|\psi_{2s}(0)|^2\,.$$

Here, $\omega_0^{\rm ex}$ includes processes in which the $1s$ or $2s$ electron is captured and the remaining electron is not in a $1s'$ or $2s'$ state in ^{7}Li. These processes are not properly K or L capture, but nonetheless lead to nuclear γ rays if the transition is to the 477.4-keV state.

For the purposes of calculation of the overlap integrals, tabulated wave functions[18] were used. These give slightly different values for the screening ratio (0.32 as compared to Winter's value of 0.26), but have been consistently used throughout the calculation of the exchange-overlap corrections. As a check, $X^{L/K}$ was computed to be 3.5 using the wave functions, in reasonable agreement with the previously quoted value of 3.7. A_{1s}, B_{1s}, and B_{2s} were computed as described in Ref. 15, and A_{2s} was taken as unity. This last approximation is valid as A_{1s} differs from unity by only 2% over the range 50–380 keV, and A_{2s} is expected to show even a smaller variation.

The predominant effect of these corrections is to increase the total intensity of $2s$ capture relative to $1s$ capture by a factor of 2.9; while the value of $\omega_{1s}/\omega_\gamma$ is decreased by 7%. However, the net effect on the ratio $\omega_{\rm IB}/\omega_\gamma$ is negligibly small, i.e., the change is less than 1%. Changes in the shape of the spectrum at energies above 50 keV are negligible, as the values of B_{1s} and B_{2s}, and of A_{1s} and A_{2s} are approximately equal over the range of energies considered.

---

†Work performed under the auspices of the U. S. Atomic Energy Commission. Work prepared under Contract No. AT(04-3)-63 for the San Francisco Operations Office, U. S. Atomic Energy Commission.

[1]P. Morrison and L. Schiff, Phys. Rev. 58, 24 (1940).

[2]R. J. Glauber and P. C. Martin, Phys. Rev. 104, 158 (1956).

[3]P. C. Martin and R. J. Glauber, Phys. Rev. 109, 1307 (1958).

[4]*Proceedings of the Conference of the Electron Capture and Higher Order Processes in Nuclear Decays*, edited by D. Berényi (Eötvös Lorand Physical Society, Budapest, 1968), Vol. II.

[5]*Proceedings of the International Conference of the*

Role of Atomic Electrons in Nuclear Transformations (Nuclear Energy Information Center of the Polish Government, Warsaw, Poland, 1963), Vol. IV.
[6]I. Kadar, D. Berényi, and B. Myslek, Nucl. Phys. A153, 383 (1970).
[7]H. Lancman and J. Lebowitz, Phys. Rev. 188, 1683 (1969).
[8]H. Lancman and J. Lebowitz, Phys. Rev. C 3, 188 (1971).
[9]H. Lancman and J. Lebowitz, Phys. Rev. C 3, 465 (1971).
[10]J. C. Vanderleeden, F. Boehm, and E. D. Lipson, Phys. Rev. C 4, 2218 (1971).
[11]J. H. Hubbell, National Bureau of Standards Report No. NSRDS-NBS29, 1969 (unpublished).
[12]A. H. Wapstra and N. B. Grove, Nucl. Data A9, 265 (1971).
[13]G. Winter, Nucl. Phys. A113, 617 (1968).
[14]J. Bahcall, Nucl. Phys. 71, 267 (1965).
[15]The relativistic correction to the 1*s* contribution was calculated using formulas (3.16a), (4.3a), (4.3b), and (4.4) of Ref. 3, while the relativistic correction to the 2*s* contribution was calculated using formulas (9.16), (9.23), and (9.25) of Ref. 2.
[16]H. Lancman, private communication.
[17]H. W. Johlige, D. C. Aumann, and H.-J. Born, Phys. Rev. C 2, 1616 (1970).
[18]F. Herman and S. Skillman, *Atomic Structure Calculations* (Prentice-Hall, Englewood Cliffs, N. J., 1963).

PHYSICAL REVIEW C VOLUME 5, NUMBER 5 MAY 1972

Variational Approach to the Bound-State Faddeev Equations

Edward Harms
Physics Department, Fairfield University, Fairfield, Connecticut 06430
(Received 19 August 1971)

A variational principle for the bound-state Faddeev equations is given. This principle takes the form of a variational expression for the linear eigenvalues of the Faddeev kernel. The variational expression is investigated for the case in which the wave function is expanded in terms of known functions. In this case it can be reduced to the variational method of Rosenberg, and hence the energies obtained are variational upper bounds for the bound-state energy. The variational expression is also used to generate a new set of one-dimensional integral equations for the bound-state problem.

I. INTRODUCTION

The usefulness of variational methods for computations on the three-nucleon bound-state system has been emphasized by Delves.[1] If one is dealing with an interaction which is derived from a potential, the Rayleigh-Ritz quotient for the energy may be taken as the variational expression of the Schrödinger equation. Many calculations have been performed using this method,[2] the most extensive and definitive being the work of Hennell and Delves and Hu[3] using the Hamada-Johnston potential[4]; and of Jackson, Landé, and Sauer[5] using the Reid potential.[6] The variational principle is also useful in suggesting approximate methods of solution, examples being the Hartree-Fock equations for many-body systems[7] and the equivalent two-body methods of Bodmer and Ali,[8] and Feshbach and Rubinow.[9]

In his study of three-particle scattering, Faddeev[10] has given a reformulation of the three-body problem in terms of two-body t matrices rather than potentials. Such modifications are essential for treating scattering phenomena[11] and at the same time offer an alternative form for the bound-state problem. This formulation has often been favored in the three-nucleon system for conceptual as well as aesthetic reasons, among them being the difficulties encountered in trying to determine the two-nucleon potential and the closer relationship between the t matrix and experiment. In addition, recent work[12] has shown how to modify the off-shell two-body t matrix directly, without the necessity of going through a potential. For such interactions the Faddeev approach seems the more natural one.

Whether the Faddeev formulation of the three-nucleon bound-state problem is more amenable to solution than the Schrödinger form is not well known. For separable potentials both methods are equivalent and easily yield solutions.[13] There have been a number of attempts at solving the Faddeev equations with local potentials. Osborn,[14] Malfliet, and Tjon,[15] and Kim and Tubis[16] have been able to solve the two-dimensional integral equations that arise when the Faddeev equations are taken into the momentum representation. The most definitive result here is that of Malfliet and Tjon with the Reid potential.

In this paper we develop a variational principle